Journal of Orthopaedic Surgery and Research

RESEARCH

Open Access

A-485 alleviates postmenopausal osteoporosis by activating GLUD1 deacetylation through the SENP1-Sirt3 signal pathway

Yinghong Ma[1,2], Xiaohua Zou[1,3,4*], Qianhong Jian[2], Jiaxin Dong[2], Xianbing Huang[2], Yue Zhai[2] and Li Qian[2,5*]

Abstract

Objective Postmenopausal osteoporosis (OP) is a bone disease caused by estrogen deficiency. A-485 is a selective inhibitor of p300/CBP histone acetyltransferase (HAT) with potential regulatory effects on bone remodeling. This study aims to investigate the effects of A-485 on postmenopausal OP and its underlying mechanisms.

Methods For animal experiments, 61 female Wistar rats were used to establish an OP model through ovariectomy (OVX). The rats were administered with A-485 (100 mg/kg/day) via intraperitoneal injection for six weeks. Bone mineral density (BMD) was measured using dual-energy X-ray absorptiometry (DXA). Histopathological changes were observed using HE and Masson's trichrome staining. ELISA was used to measure bone resorption markers (CTX-1, DPD) and the bone formation marker (P1NP) in rats. Osteoblast differentiation markers (Runx2, OCN), SENP1, Sirt3 expression levels, and GLUD1 acetylation were assessed via Western blot (WB) and RT-qPCR. In vitro, MC3T3-E1 osteogenic progenitor cells were cultured in osteogenic differentiation medium supplemented with ascorbic acid, β-glycerophosphate, dexamethasone, and fulvestrant. CCK-8 was performed to evaluate cell proliferation. Flow cytometry was selected to measure apoptosis and mitochondrial membrane potential. WB and RT-qPCR were employed to analyze ERα, ERβ, Runx2, Sirt3, and GLUD1 acetylation. Additionally, Alizarin red staining was applied to monitor osteoblast mineralization. ATP levels were detected using a commercial kit, and ROS levels were measured by MitoSOX Red.

Results In vivo, ovariectomized rats exhibited lower BMD, impaired bone trabeculae, increased CTX-1 and DPD, and altered expression of Runx2 and OCN, all of which were reversed by A-485 treatment. In vitro, A-485 activated GLUD1 deacetylation, enhanced osteogenic differentiation, and improved mitochondrial function. Regarding the mechanism, A-485 activated the SENP1-Sirt3 signal pathway, with SENP1 knockdown negating the effects of A-485. In vivo, A-485 reduced GLUD1 acetylation and promoted improvement of OP, which were reversed by SENP1 knockdown.

Conclusion A-485 ameliorates postmenopausal OP by activating GLUD1 deacetylation via the SENP1-Sirt3 signal pathway, thus improving mitochondrial function, and promoting osteogenic differentiation and mineralization.

Keywords A-485, SENP1-Sirt3 signal pathway, GLUD1, Osteoporosis

*Correspondence:
Xiaohua Zou
zouxiaohuazxh@gmc.edu.cn
Li Qian
wsql-bio@163.com

Full list of author information is available at the end of the article

Introduction

Postmenopausal osteoporosis (OP) is a prevalent and severe health condition primarily caused by the accelerated bone density loss and increased bone fragility due to estrogen deficiency [1, 2]. Current therapeutic strategies for postmenopausal OP mainly include bisphosphonates [3, 4], selective estrogen receptor modulators, estrogen therapy, and parathyroid hormone administration [5, 6]. However, the clinical utility of these treatments is limited by challenges in administration and adverse effects, which often lead to poor patient compliance [7].

A-485, a high-selective acetylase inhibitor [8], has demonstrated therapeutic potential in cancer treatment and metabolic disorders [9]. A recent study indicated that A-485 also holds promise for treating OP [10]. Its precise targeting and fewer side effects make it a promising candidate for OP therapy [11]. However, the precise mechanisms by which A-485 exerts its effects in OP remain unclear. Notably, A-485 has been reported to regulate key metabolic enzymes [12], potentially including glutamate dehydrogenase 1 (GLUD1) [13]. GLUD1 is a mitochondrial enzyme crucial for energy production [14], and its acetylation level directly impacts mitochondrial function [15]. Given that mitochondrial dysfunction is closely linked to the pathogenesis of OP [16], impaired mitochondrial function results in insufficient energy supply, limiting osteoblast differentiation and bone matrix synthesis, which leads to severe bone loss [17]. Therefore, A-485 may exert therapeutic effects in OP by improving mitochondrial function through GLUD1 deacetylation.

The SUMO-specific protease 1 (SENP1)-Sirtuin 3 (Sirt3) signal pathway is a key regulator of cellular mechanisms that influences cellular metabolism, mitochondrial function, and stress response through acetylation modifications [18, 19]. Zhou W et al. demonstrated that the SENP1-Sirt3 signal pathway can regulate GLUD1 activity [20]. This pathway is particularly important in regulating protein acetylation, which plays a pivotal role in controlling mitochondrial function [21]. Impaired mitochondrial function is a hallmark of OP [22], and modulation of this pathway by A-485 could lead to GLUD1 deacetylation, improving mitochondrial function and alleviating OP symptoms. The potential modulation of this pathway by A-485 could enhance mitochondrial energy production and reduce oxidative stress [23], both of which are crucial for maintaining bone health and preventing the bone loss characteristic of OP. To support our research hypothesis, we propose that A-485 may regulate GLUD1 deacetylation through the SENP1-Sirt3 signaling pathway, improving mitochondrial function and alleviating OP symptoms. SENP1, as a SUMO-specific protease, regulates protein desumoylation and acetylation, directly affecting cellular metabolism and mitochondrial function. Sirt3, through deacetylation, regulates mitochondrial energy metabolism. Studies have shown that the SENP1-Sirt3 signaling pathway plays a crucial role in regulating GLUD1 activity, and GLUD1 deacetylation helps improve mitochondrial function, promoting the normal function of osteoblasts. Therefore, we hypothesize that A-485 may improve mitochondrial function and slow the progression of osteoporosis by modulating this signaling pathway.

Taken together, this study aimed to investigate the therapeutic potential of A-485 in postmenopausal OP, with a specific focus on its regulation of GLUD1 deacetylation via the SENP1-Sirt3 signal pathway. The findings may provide a theoretical foundation for the clinical application of A-485 and help develop new treatment strategies for OP.

Methods

Animal treatment and grouping

Forty-Eight female Wistar rats (3 months old, 220–260 g) were purchased from Trophic Biomart (Nantong, Jiangsu, China). Prior to experimentation, the rats were acclimatized in a specific pathogen-free (SPF) environment with controlled constant temperature (20–24℃), humidity (45–60%), and a standard 12-h light/dark cycle for 7 d. The rats were randomly assigned to six groups: Sham, Model, Model + A-485, Model + A-485 + sh-NC and Model + A-485 + sh-SENP1. Regarding the ovariectomy (OVX) procedure, all surgical instruments were sterilized using ultraviolet light. Anesthetize rats. A 1.5 cm midline dorsal incision was made, followed by bilateral muscle incisions to expose and excise the ovaries. The incisions were closed with sutures. In the Sham group, an equivalent amount of adipose tissue was removed instead of the ovaries. Postoperative recovery lasted for 3 weeks. In the A-485 treatment groups, rats were administered A-485 at 100 mg/kg/d by intraperitoneal injection for 6 weeks. Rats in the Sham and Model groups received equivalent volumes of saline [24, 25]. This study was approved by The Animal Ethics Committee of Guizhou Medical University (Ethics Approval Number:2023070110).

Cell treatment and grouping

Pretreated MC3T3-E1 cells were seeded at 3×10^4 cells/well onto glass coverslips in 24-well plates and cultured in osteogenic medium containing 50 μg/mL ascorbic acid (50-81-7, Sigma-Aldrich), 10 mM β- glycerophosphate (154804-51-0, Sigma-Aldrich), and 10 nM dexamethasone (50-02-2, Sigma-Aldrich). The cells were randomly divided into six groups: Control, Model, Model + A-485, Model + A-485 + sh-NC, Model + A-485 + sh-SENP1 group, and Model + A-485 + SAHA. The Control group received continuous supplementation with 10 nM estradiol. All other Model groups were cultured under estrogen-deprived conditions and treated with 100 nM of the

selective estrogen antagonist Fulvestrant (129453-61-8, Sigma-Aldrich) to neutralize residual estrogen in the fetal bovine serum (FBS), effectively simulating osteoporotic conditions [26].

Plasmid construction and transfection

The short hairpin RNA (shRNA) sequence targeting SENP1 (CCAGCCTATCGTCCAGATTATCTCGAG ATAATCTGGACGATAGGCTGG) was cloned into pLKO.1 vector (V010449, Novopro, Shanghai, China) to construct sh-SENP1 plasmid. For in vitro transfection, MC3T3-E1 cells were seeded into 96-well plates with 3×10^4 cells per well. When cell confluence reached 90%, transfection was performed using Lipofectamine 3000 transfection reagent diluted in Opti-MEM medium (51985091, Thermo Fisher, Massachusetts, USA) with either the sh-SENP1 plasmid or a scrambled shRNA negative control (sh-NC; SIC001, Sigma-Aldrich). The plasmid-transfection reagent mixture was incubated at 37℃ for 20 min. The incubated mixture was then added to cell culture wells and incubation was continued at 37 °C for 48 h. For in vivo transfection, the plasmid-transfection reagent complex was directly injected into cartilage tissue using a fine needle.

Bone densitometry

Bone mineral density (BMD) of the lumbar spine and whole body was measured using dual-energy X-ray absorptiometry (DXA) with a Hologic 4500 (Waltham, MA, United Kingdom) bone densitometer. All procedures were performed in strict accordance with the manufacturer's protocols.

Hematoxylin-eosin (HE) and Masson's trichrome staining

Euthanasia was performed by intraperitoneal injection of 150 mg/kg 2% sodium pentobarbital (P3761, Sigma-Aldrich), as approved by the Ethics Committee of Guizhou Medical University (Ethics Approval Number:2023070110).

Subsequently, cartilage tissue was immediately harvested, fixed with tissue fixative (MA0192, Meilune, Dalian, China), and embedded in paraffin. The tissue was then sectioned to a thickness of 4 μm. After deparaffinization and rehydration, the sections were stained with hematoxylin using HE staining kit (C0105S, Beyotime, Shanghai, China), rinsed, and then stained with acidic ethanol. After this, the sections were blued in alkaline water, counterstained with eosin, rinsed, and dehydrated through an ethanol gradient. Following dehydration, the sections were cleared in xylene and sealed with a mounting medium (C0187, Beyotime).

Additionally, Masson's trichrome staining was performed using a Masson staining kit (C0189S, Beyotime) according to the manufacturer's instructions. Briefly, nuclei were stained with ferric hematoxylin, followed by differentiation with acidic alcohol and treatment with phosphomolybdic acid to enhance the staining effect. The sections were stained with magenta to visualize muscle, cytoplasm, and collagen fibers. After further differentiation with phosphotungstic acid, the sections were stained with aniline blue or bright green to color the collagen fibers blue or green, respectively. Finally, the sections were dehydrated, cleared with xylene, and mounted for microscopic observation.

Cartilage histopathology was observed using a light microscope (CX43, Olympus, Japan), and the tissue damage was analyzed based on the microscopic images.

Enzyme linked immunosorbent assay (ELISA)

Frozen cartilage tissue samples were placed in PBS (10010023, Thermo fisher) buffer at a 1:10 ratio and homogenized using a homogenizer. The homogenate was then lysed on ice for 30 min to extract proteins, during which a protease inhibitor (HY-K0011, Medchem express, Monmouth, NJ, USA) was added to prevent protein degradation. Subsequently, the samples were centrifuged at 4℃ for 15–20 min to remove cell debris and unlysed tissue, and the supernatant was collected as the protein extract. The levels of several biomarkers, including carboxy-terminal cross-linked telopeptide of type 1 collagen (CTX-1) (E-EL-M3023, elabscience, Wuhan, China), deoxypyridinoline (DPD) (MBS261900, biocompare, Shanghai, China) and procollagen type 1 N- terminal propeptide (P1NP) (D721053, sangon, Shanghai, China) were measured using the respective ELISA kits. All procedures were carried out following the manufacturer's instructions.

Western blot (WB) analysis

MC3T3-E1 cells were lysed using RIPA lysis buffer (ab170197, Abcam, Cambridge, UK), and total protein was collected. Protein concentration was determined using the BCA Protein Quantification Kit (P0010, Beyotime). Equal amounts of protein samples were separated by SDS-PAGE and transferred onto PVDF membranes (ab133411, Abcam) using the wet transfer method. Subsequently, the membranes were incubated overnight at 4℃ with the primary antibodies against Runx2 (1:1000, ab236639, Abcam), OCN (1:100, ab93876, Abcam), Estrogen Receptor alpha (ERα) (1:1000, ab92516, Abcam), Estrogen receptor beta (ERβ) (1:1000, ab22595, Abcam), Acetyl Lysine (1:1000, ab190479, Abcam), GLUD1 (1:500, ab153973, Abcam), ALP (1:500, ab153973, Abcam), and GLUD1 (1:500, ab153973, Abcam), ALP (1:1000, ab307726, Abcam), SENP1 (1:500, ab236094, Abcam), Sirt3 (1:1000, ab217319, Abcam), and GAPDH (1:10000, ab181602, Abcam). After washing the membranes, they were incubated with a secondary antibody (1:1000,

ab6702, Abcam) for 2 h. The membranes protein bands were developed using ECL (A38554, Thermo fisher), and the grayscale values were analyzed using Image J software (V1.8.0.112, NIH, Madison, WI, USA).

Reverse transcription quantitative polymerase chain reaction (RT-qPCR)

Total RNA was extracted from each group of MC3T3-E1 cells using a Rapid RNA Extraction Kit (IPD-X075, Ipodix, Wuhan, China), which was reverse-transcribed to cDNA using a Reverse Transcription Kit (K1691, Thermo fisher). The mRNA expression was detected using an RT-qPCR system. GAPDH was used as an internal reference gene, and the primer sequences are shown in Table 1. The PCR experiments were repeated three times, with three replicate wells each time. Relative mRNA expression was calculated by the qPCR algorithm (Relative Quantification, $2^{-\Delta\Delta Ct}$ method).

Cell counting kit-8 (CCK-8) assay

The CCK-8 kit (C0037, Beyotime) was used to assess MC3T3-E1 cell proliferation assay. Cells were seeded into 96-well plates at 3×10^3/well. At 0, 24, and 48 h, respectively, each well was loaded with 10 μL of CCK-8 reagent and 90 μL of complete medium, followed by incubation at 37 °C for 2 h. Absorbance was then measured at 450 nm using a microplate reader (Gen5, BioTek, Winooski, VT, United States).

Flow cytometry

Apoptosis rates were analyzed using the Annexin V-FITC/PI Apoptosis Kit (A8604-200UL, Merck, Darmstadt, Germany). After 24 h of treatment in 6-well plates, cells were resuspended in 500 μL binding buffer. To stain the cells, 5 μL of FITC-Annexin V and 10 μL of PI were added, and the cells were incubated for 15 min at room temperature in the dark. Following staining, the cells were analyzed using a flow cytometer (Moflo XDP, USA). Early apoptotic cells were identified as Annexin V positive and PI negative, while late apoptotic cells were both Annexin V and PI positive. The results were expressed as the percentage of apoptotic cells.

Table 1 Primer sequences used for qPCR analysis

Gene	Direction	Sequence (5′-3′)
ERα	F	CTTTTGAACCAGCAGGGTGGC
	R	GAAGGGTCATGGTCATGGTCAG
ERβ	F	ACTGCTGAGCACCTTGAGTC
	R	CCCCTCATCCCTGTCCAGAA
Runx2	F	TTCATTCGCCTCACAAACAACC
	R	CTTGCAGCCTTAAATGACTCGG
OCN	F	CCGTTTAGGGCATGTGTTGC
	R	TCGAGTCCTGGAGAGTAGCC
SENP1	F	CGGTTCCGGTTCGGATTTTG
	R	TTGAGGTCTTCCGGGTTTCG
Sirt3	F	CAGCGGCTCCCCAAAGAACAC
	R	CGGCTCTACACGCAGAACATC
GAPDH	F	CATCACCATCTTCCAGGAGCGA
	R	TGGTTCACACCCATCACAAACA

JC-1 detection of mitochondrial membrane potentials

MC3T3-E1 cells were incubated with JC-1 staining solution (C2006, Beyotime) for 10 min at 37℃, followed by three washes with buffer. The data were then detected and analyzed using fluorescence microscopy (CX43, Olympus). In healthy mitochondria, JC-1 aggregates emitted red fluorescence (excitation: 585 nm, emission: 590 nm), whereas in depolarized mitochondria, JC-1 monomers emitted green fluorescence (excitation: 514 nm, emission: 529 nm). The red-to-green fluorescence ratio (H1-UL/H1-UR) was used to assess changes in mitochondrial membrane potential (ΔΨm).

Isolation of mitochondria-enriched fractions

Mitochondria-enriched fraction were isolated from MC3T3-E1 cells. Briefly, cells were collected from culture flasks and centrifuged for 15 min. The pellet was resuspended in a buffer containing 0.25 M sucrose, 0.15 M KCl, 10 mM Tris-HCl pH 7.4 (ST774, Beyotime) and 1 mM EDTA (R1021, Thermo fisher). The suspension was then centrifuged for 15 min, and the mitochondrial pellet was resuspended in the same buffer [27].

Immunoprecipitation (IP)

Cells were lysed using a cell lysis buffer containing Tris-HCl (RES3098T-B7, Sigma aldrich), NaCl (204439, Sigma aldrich), EDTA (03609, Sigma aldrich), Triton X-100 (X100, Sigma aldrich), glycerol (G5516, Sigma aldrich), double-distilled water, and protease inhibitors (GRF101, Epizyme, Shanghai, China). The lysates were cleared by incubation with Protein A/G agarose beads (sc-2003, Santa Cruz, SC, USA) for 0.5 h at 4℃. The supernatant was then incubated with a GLUD1-specific antibody (ab166618, Abcam) at 4℃ overnight. The next day, the suspension was incubated with protein A/G agarose beads for 2 h at 4 °C. The immunoprecipitated complexes were washed with cell lysis buffer and subjected to WB.

Alizarin red S (ARS) staining

MC3T3-E1 cells were stained with ARS. Briefly, before staining, cells were fixed in 4% paraformaldehyde (MA0192, Meilune, Dalian, China) for 20 min at room temperature, washed twice with distilled water, and then stained with 500 μL ARS solution (C0138, Beyotime) for 2 h at room temperature. Stained cells were visualized using a light microscope (CX43, Olympus).

Determination of mitochondrial adenosine triphosphate (ATP) synthesis

Mitochondrial ATP synthesis was assessed before and after exposure to an 808 nm laser. The samples were incubated in a reaction solution containing 100 mM Tris-HCl (ST774, Beyotime), 100 mM KCl, 1 mM EGTA (R1021, Thermo fisher), 2.5 mM EDTA (R1021, Thermo fisher), 5 mM $MgCl_2$ (7786-30-3, Chemical book, Beijing, China), 0.2 mM di (adenosine-5′) penta-phosphate, 0.6 mM ouabain (11018-89-6, Medchem express), 25 μg/mL ampicillin (69-53-4, Medchem express), 5 mM KH_2PO_4 (7758-11-4, Chemical book), 5 mM pyruvate (P2256, Sigma aldrich), and 2.5 mM malate (442610-M, Sigma aldrich) as respiratory substrates. After incubation, ATP synthesis was initiated by adding 0.1 mM ADP. ATP production was monitored for 2 min using a luminometer through the luciferin/luciferase chemiluminescence method [15]. The results were calibrated using ATP standard solutions ranging from 10^{-9} to 10^{-7} M.

Detection of mitochondrial reactive oxygen species (ROS)

MC3T3-E1 cells were incubated with 5 μM MitoSOX™ Red (M36008, Thermo Fisher) dye for 10 min at 37℃, protected from light. Oxidized MitoSOX Red binds to nucleic acids in the mitochondria, producing intense red fluorescence with an excitation wavelength of 510 nm and an emission wavelength of 580 nm. Additionally, the cells were stained with Hoechst dye (33342, Thermo Fisher) for 10 min to label the nuclei. After staining, fluorescent signals were detected using a fluorescence microscope (Olympus), with MitoSOX Red indicating the mitochondria and Hoechst labeling nuclei.

Statistical analysis

GraphPad Prism9 (Dotmatics, Boston, MA, USA) software was used for statistical analysis. Student's *t*-test was applied to compare data data between two groups, while one-way analysis of variance (ANOVA) was used for comparisons involving three and more groups, followed by Tukey's post-hoc comparisons. Two-way ANOVA was used to assess the the effects of multiple factors on a continuous dependent variable. A *p*-value less than 0.05 was considered statistically significant. Each experiment was repeated at least three times.

Results

A-485 alleviates OP-related symptoms in ovariectomized rats

OP is characterized by reduced BMD, deteriorated bone microarchitecture, and increased fracture risk [28]. Consistent with these hallmarks, DXA revealed a significant reduction in BMD in the Model group compared to the Sham group. Notably, BMD was significantly restored in the Model + A-485 group compared to the Model group (Fig. 1A, $p < 0.0001$). In cartilage tissue staining, the Sham group showed intact, tightly arranged bone trabeculae with regular morphology, exhibiting a compact trabecular structure and uniform, abundant collagen fiber distribution. In contrast, the Model group displayed significantly thinned and broken trabeculae, with uneven and reduced collagen fiber distribution. The staining intensity of the trabeculae was noticeably diminished, with a marked reduction in the blue area and a weakened red coloration in the matrix. Additionally, an increase in adipose tissue within the bone marrow cavity was observed, indicative of fat accumulation associated with the disease state. After A-485 treatment, the damage to the trabeculae was mitigated, the extent of trabecular disruption was reduced, and collagen fiber distribution was partially restored. Moreover, the adipose tissue in the bone marrow cavity decreased, suggesting a potential role of A-485 in modulating fat content in addition to its protective effects on bone structure (Fig. 1B). Biochemical markers also confirmed OP progression in ovariectomized rats. The serum level of CTX-1 in the Sham group was 0.09 ng/mL, while the OVX group showed a significant increase to 0.50 ng/mL. The P1NP level in the Sham group was 20.12 μg/L, which decreased to 12.23 μg/L in the OVX group. The urinary DPD level in the Sham group was 10.12 nM, which increased to 71.79 nM in the OVX group. After A-485 treatment, CTX-1 (0.22 ng/mL) and DPD (52.24 nM) levels were decreased compared to the OVX group and P1NP levels were increased (18.71 μg/L) (Fig. 1C). Furthermore, WB and RT-qPCR indicated that, compared to the Sham group, the mRNA and protein expression levels of osteogenic differentiation markers Runx2 and OCN were reduced in the Model group. After A-485 treatment, the levels of Runx2 and OCN were significantly rescued in ovariectomized rats (Fig. 1D-E, $p < 0.001$). These findings suggest that A-485 can effectively alleviate OP progression in ovariectomized rats.

A-485 inhibits mitochondrial protein acetylation in MC3T3-E1 cells

Existing evidence has shown that A-485 inhibits protein acetylation levels [20], but whether it improves OP by regulating protein acetylation remains unclear. Our in vitro results demonstrated that, compared to the Control group, the Model group exhibited reduced cell proliferation (Fig. 2A, $p < 0.001$), a significant increase in apoptosis rate from 10.23 to 34.47% (Fig. 2B, $p < 0.0001$), decreased expression of estrogen receptors ERα and ERβ, and lowered levels of osteogenic markers Runx2 and OCN (Fig. 2C-D, $p < 0.0001$). After A-485 treatment, cell proliferation was increased, ERα and Erβ levels were restored, and the expression of Runx2 and OCN was upregulated, alongside a reduction in apoptosis (23.70%).

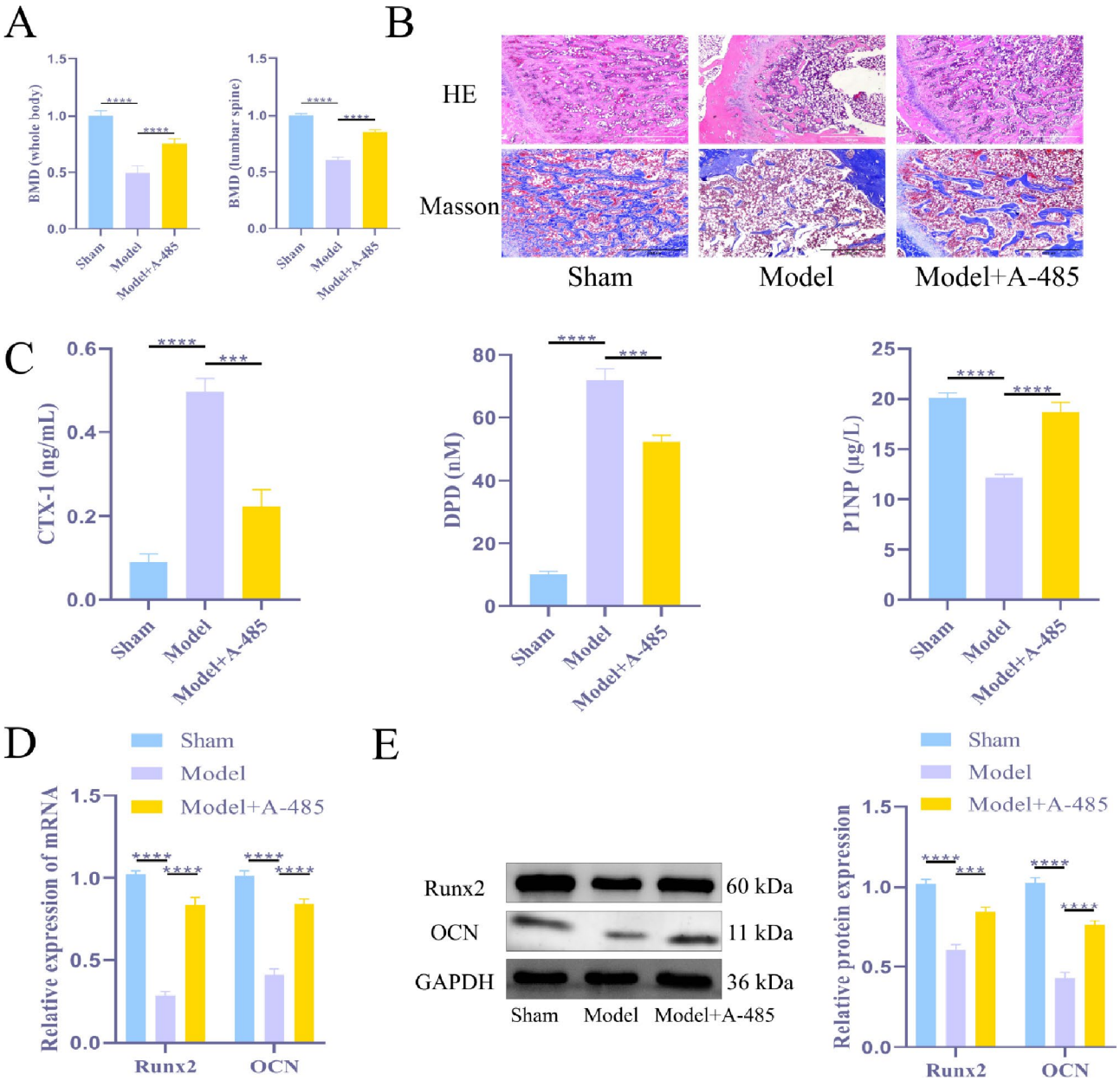

Fig. 1 Effect of A-485 on OP-like symptoms in ovariectomized rats. (**A**) Measurement of bone mineral density (BMD) using DXA. (**B**) HE and Masson's trichrome staining images of trabecular structure and damage. (**C**) Detection of serum levels of CTX-1 and P1NP, and urinary levels of DPD. (**D**) RT-qPCR analysis of mRNA expression levels of Runx2 and OCN. (**E**) WB analysis of protein expression levels of Runx2 and OCN. $N=6$; ns, $p>0.05$; ***, $p<0.001$, ****, $p<0.0001$

These findings indicate that the in vitro OP-like model was successfully constructed and A-485 could improve osteogenic differentiation and promote estrogen receptor expression.

Additionally, compared to the Control group, the acetylation levels of mitochondrial proteins were elevated in the Model group, while there was no significant change in the acetylation levels of non-mitochondrial proteins. After A-485 treatment, the acetylation levels of mitochondrial proteins were normalized, without affecting the acetylation levels of non-mitochondrial proteins (Fig. 2E). The results suggest that A-485 improves osteogenic differentiation and reduces the acetylation levels of mitochondrial proteins in the in vitro OP model.

A-485 promotes osteoblast differentiation and mineralization by inhibiting mitochondrial GLUD1 acetylation

We first assessed the acetylation level of mitochondrial GLUD1 in MC3T3-E1 cells across the experimental

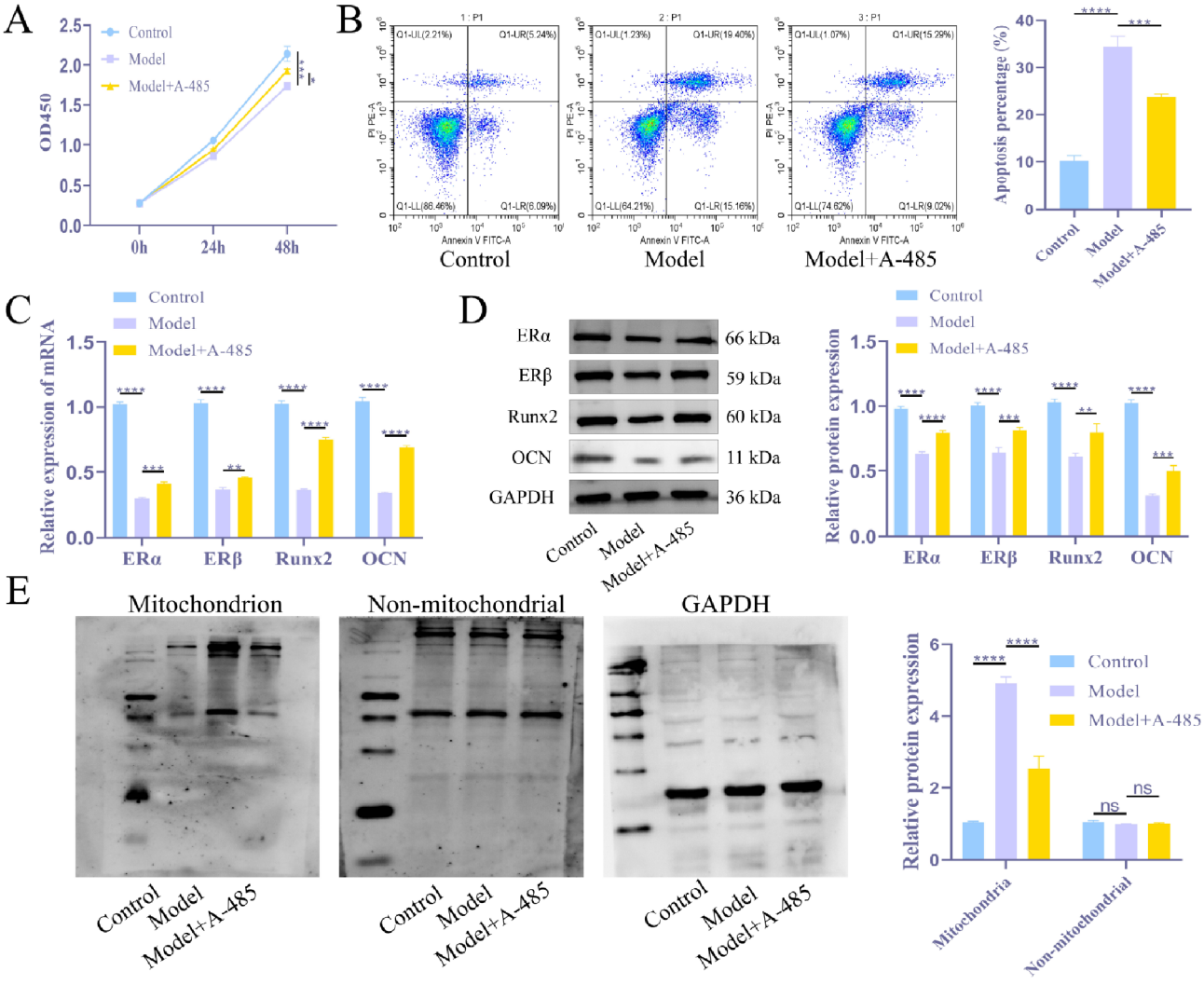

Fig. 2 Effects of A-485 on osteogenic differentiation and protein acetylation levels in MC3T3-E1 cells modeled by estrogen deprivation. (**A**) CCK-8 assay to detect cell proliferation capacity. (**B**) Flow cytometry to assess cell apoptosis rate. (**C**) RT-qPCR to measure mRNA expression levels of ERα, ERβ, Runx2, and OCN. (**D**) WB analysis to detect protein expression levels of ERα, ERβ, Runx2, and OCN. (**E**) WB analysis to examine acetylation levels of mitochondrial and non-mitochondrial proteins. $N = 3$; ns, $p > 0.05$; *, $p < 0.05$; **, $p < 0.01$; ***, $p < 0.001$, ****, $p < 0.0001$

groups. IP results showed that GLUD1 acetylation was significantly elevated in the Model group compared to the Control group, which was rescued following A-485 treatment. This therapeutic effect was abrogated by the addition of SAHA, confirming HDAC-dependent resurgence of GLUD1 acetylation (Fig. 3A, $p < 0.0001$).

With regard to the MC3T3-E1 cell status, compared to the Control group, the Model group exhibited lower levels of Runx2 and OCN (Fig. 3B-C, $p < 0.0001$), along with decreased cell mineralization (Fig. 3D). Treatment with A-485 reversed the damage to MC3T3-E1 cells, restoring Runx2 and OCN while enhancing mineralization. Pharmacological inhibition via SAHA co-treatment abolished these benefits (Fig. 3D). These results mechanistically link A-485's anti-osteoporotic effects to mitochondrial GLUD1 deacetylation, which promotes osteoblast differentiation and mineralization.

A-485 alleviates mitochondrial dysfunction by inhibiting GLUD1 acetylation

Quantitative analysis revealed that, compared to the Control group, GLUD1 acetylation levels were significantly increased in the Model group (Fig. 4A, $p < 0.0001$). Additionally, mitochondrial dysfunction was evidenced by a 71.50% decrease in ΔΨm (Fig. 4C, $p < 0.0001$), a 2.75 nmol/μL reduction in ATP levels (Fig. 4B, $p < 0.0001$), and a nearly tenfold increase in ROS production (Fig. 4D, $p < 0.0001$). In the Model + A-485 group, GLUD1 acetylation was decreased, ΔΨm increased by 36.81%, ATP levels rose by 1.69 nmol/μL, and ROS production significantly decreased, indicating that A-485 alleviated

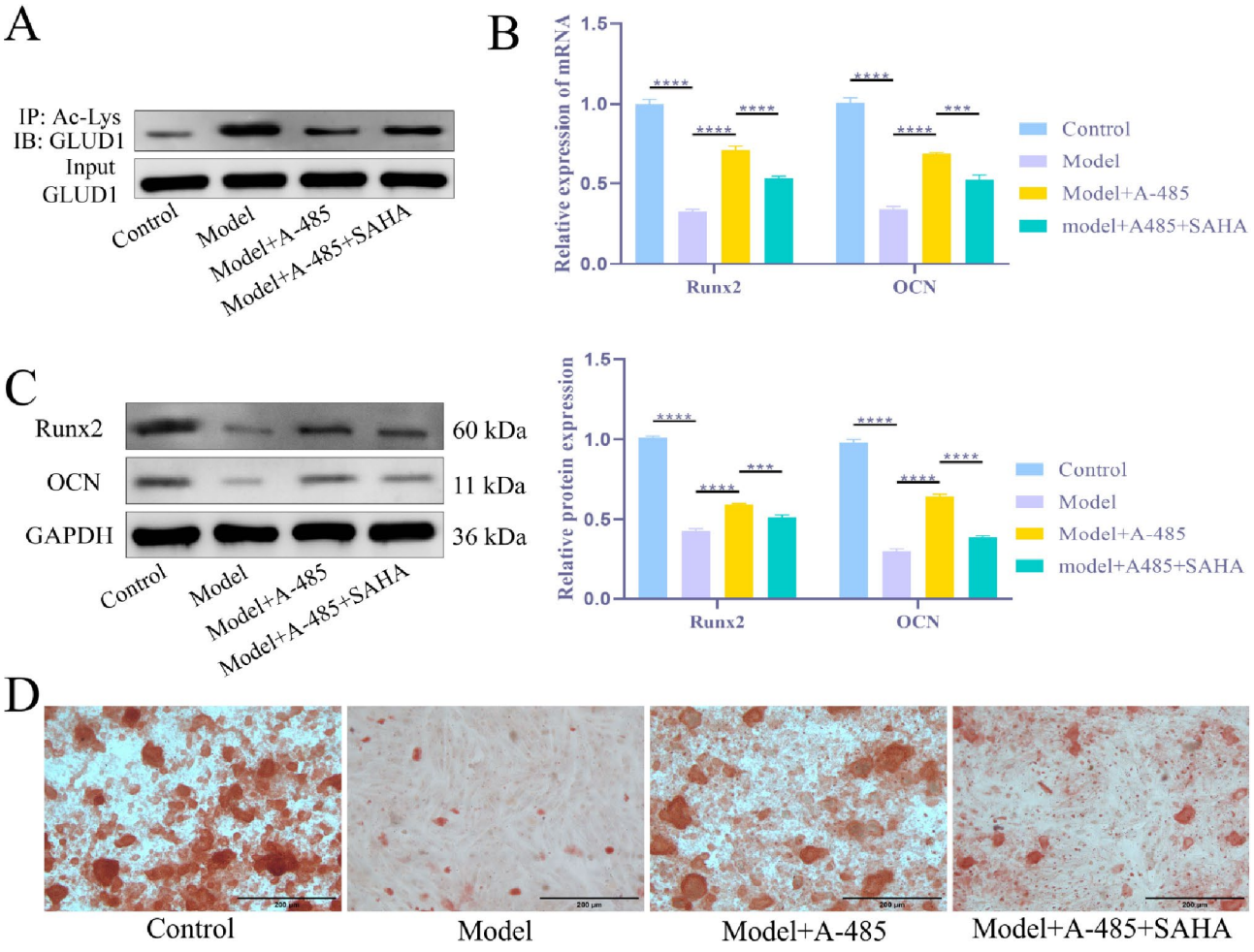

Fig. 3 Effects of A-485 on mitochondrial GLUD1 acetylation, osteogenic differentiation, and mineralization in MC3T3-E1 cells. (**A**) Co-IP analysis of GLUD1 acetylation levels. (**B**) RT-qPCR analysis of mRNA expression levels of Runx2 and OCN. (**C**) WB analysis of protein expression levels of Runx2 and OCN. (**D**) Mineralization capacity assay. $N = 3$; ***, $p < 0.001$, ****, $p < 0.0001$

mitochondrial dysfunction. Strikingly, when SAHA was added, mitochondrial function worsened compared to the Model + A-485 group, suggesting that the observed changes were specifically linked to the inhibition of GLUD1 acetylation.

A-485 promotes GLUD1 deacetylation through activation of the SENP1-Sirt3 signal pathway

The results showed that, compared to the Control group, the Model group exhibited decreased expression of both SENP1 and Sirt3. However, treatment with A-485 significantly increased the activity of these two regulators (Fig. 5A-B, $p < 0.0001$). To further validate the functional role of the SENP1/Sirt3 pathway, we knocked down SENP1 and identified sh-SENP1-3 as the most efficient knockdown construct for subsequent experiments. Notably, although A-485 treatment reduced GLUD1 acetylation levels, this effect was reversed by SENP1 knockdown (Fig. 5C). These findings indicate that A-485 promotes GLUD1 deacetylation by activating the SENP1-Sirt3 signaling pathway.

A-485 ameliorates mitochondrial dysfunction and enhances osteoblast differentiation and calcification through SENP1-Sirt3 signal pathway-mediated GLUD1 deacetylation.

We further investigated whether A-485 affects mitochondrial dysfunction, osteoblast differentiation and calcification by modulating the SENP1-Sirt3 signal pathway-mediated GLUD1 deacetylation. The results revealed that, compared to the Control group, the Model group exhibited increased GLUD1 acetylation levels (Fig. 6A, $p < 0.0001$), decreased ΔΨm (Fig. 6C, $p < 0$ 0.0001), reduced ATP levels (Fig. 6B, $p < 0.0001$), elevated ROS levels (Fig. 6D, $p < 0.0001$), downregulated Runx2 and OCN (Fig. 6E-F, $p < 0.0001$), and impaired cell proliferation and mineralization capacity (Fig. 6G). In contrast, the Model + A-485 group showed reduced GLUD1 acetylation, increased ΔΨm and ATP levels, decreased ROS production, upregulated Runx2 and

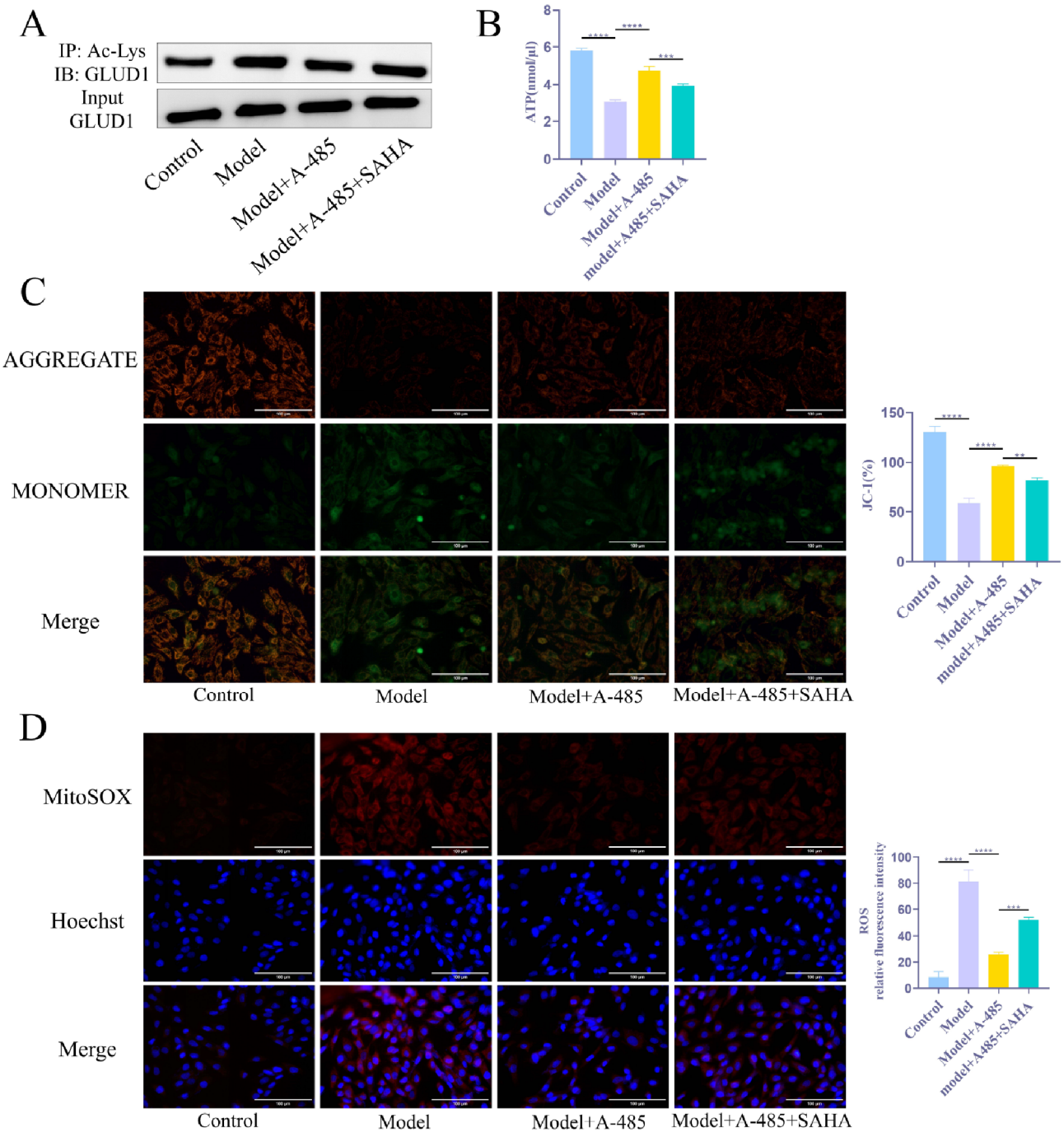

Fig. 4 A-485 alleviates mitochondrial dysfunction by inhibiting GLUD1 acetylation. (**A**) Co-IP detection of GLUD1 acetylation levels. (**B**) Detection of ATP levels. (**C**) JC-1 staining to detect mitochondrial membrane potential (ΔΨm). (**D**) Detection of ROS levels. $N = 3$; **, $p < 0.01$; ***, $p < 0.001$, ****, $p < 0.0001$

OCN expression, and enhanced cell proliferation and mineralization (Fig. 6A-G, $p < 0.0001$). However, SAHA inhibited these therapeutic effects of A-485 ($p < 0.05$). Furthermore, compared to the Model + A-485 + sh-NC group, the Model + A-485 + sh-SENP1 group displayed elevated GLUD1 acetylation, a 34.3% reduction in ΔΨm, a decrease by 0.89 nmol/μL in ATP levels, a 1.6-fold increase in ROS levels, decreased expression of Runx2 and OCN, and reduced cell proliferation and mineralization capacity ($p < 0.001$).

A-485 ameliorates OVX-induced OP through SENP1-Sirt3 signal pathway-mediated deacetylation of GLUD1

The results showed significantly decreased expressions of SENP1 and Sirt3 (Fig. 7A, C, $p < 0.0001$), and higher levels of GLUD1 acetylation in the Model group compared

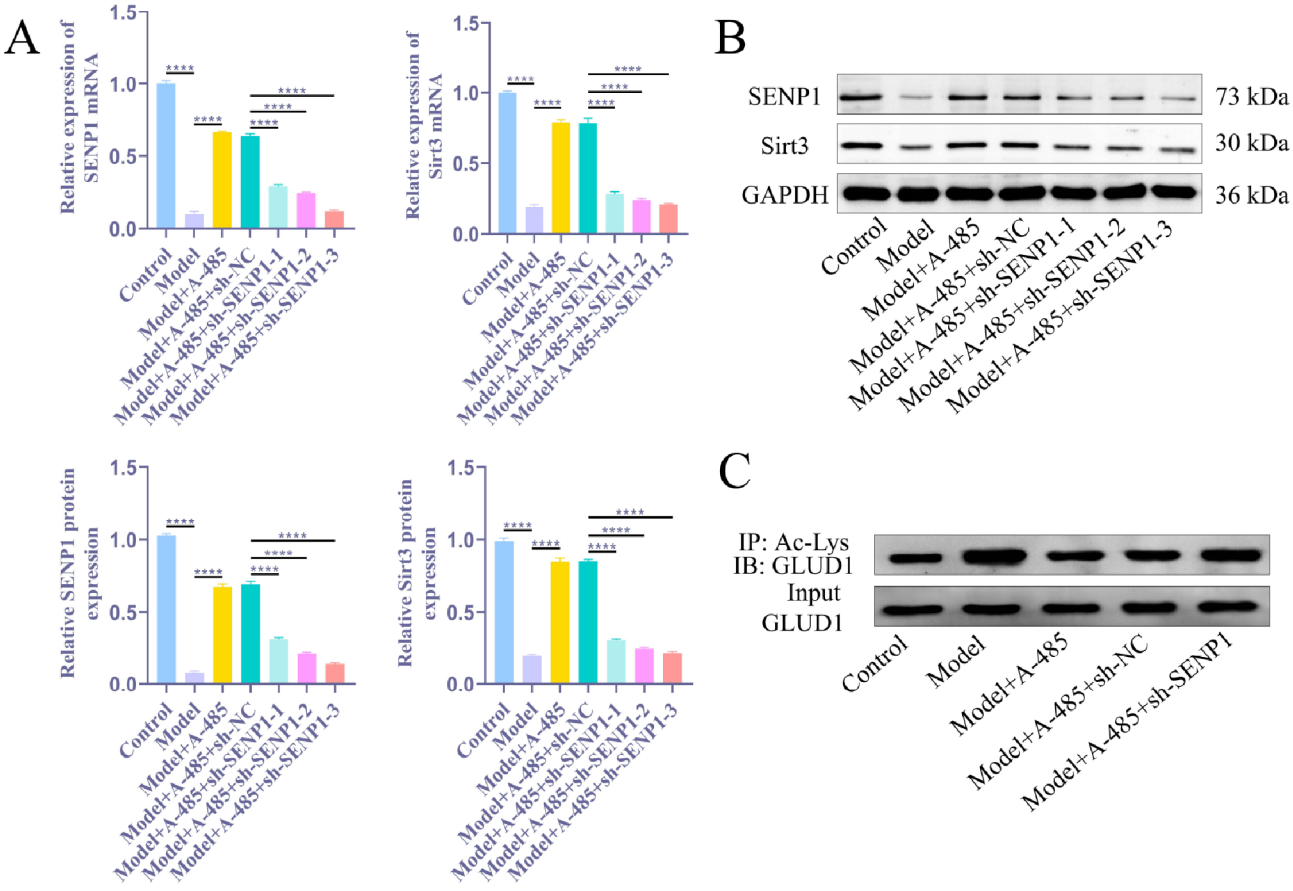

Fig. 5 A-485 promotes GLUD1 deacetylation by activating the SENP1-Sirt3 signal pathway. (**A**) RT-qPCR detection of SENP1 and Sirt3 mRNA expression levels. (**B**) WB detection of SENP1 and Sirt3 protein expression levels. (**C**) Co-IP analysis of GLUD1 acetylation levels. $N = 3$, ****, $p < 0.0001$

to the Sham group (Fig. 7B, $p < 0.0001$). Additionally, the Model group showed lower BMD (Fig. 7D, $p < 0.0001$), reduced bone trabeculae area with severe damage (Fig. 7F), elevated serum CTX-1 levels, suppressed P1NP expression, and elevated DPD levels in urine (Fig. 7E, $p < 0.0001$). Protein and mRNA expression levels of Runx2 and OCN were reduced in cartilage tissues of ovariectomized rats (Fig. 7G-H, $p < 0.0001$). Compared with the Model group, the Model + A-485 group showed reduced GLUD1 acetylation levels (Fig. 7B, $p < 0.0001$), elevated expression of SENP1 and Sirt3 (Fig. 7A, C, $p < 0.0001$), less damage to cartilage tissues (Fig. 7F), reduced CTX-1 expression, elevated P1NP levels, and reduced levels of DPD in urine (Fig. 7E). The levels of Runx2 and OCN were elevated in the cartilage tissues of treated rats (Fig. 7G-H).

In contrast, compared with the Model + A-485 + sh-NC group, the Model + A-485 + sh-SENP1 group showed significantly higher GLUD1 acetylation (Fig. 7B), lower expression of SENP1 and Sirt3 (Fig. 7A, C), lower BMD (Fig. 7D, $p < 0.0001$), severer bone trabecular damage (Fig. 7F), higher serum CTX-1 levels, lower P1NP, and higher levels of DPD in urine (Fig. 7E). The protein and mRNA levels of Runx2 and OCN were reduced in cartilage tissues (Fig. 7G-H, $p < 0.05$). These results suggest that A-485 ameliorates OP in ovariectomized rats by activating GLUD1 deacetylation through the SENP1-Sirt3 signal pathway.

Discussion

Postmenopausal OP is a chronic condition that severely compromises human health and quality of life, with a high rate of disability [29–32]. The global incidence of postmenopausal OP is rapidly increasing [33–36]. Current treatments, although capable of modestly attenuating BMD loss and fracture risk, have notable limitations [37, 38], such as inconsistent efficacy, side effects of long-term medication, and limited applicability to certain patient populations [39, 40]. Therefore, the development of novel, safe, and effective therapeutic agents for OP is essential to synergistically reduce side effects while improving therapeutic efficacy and long-term prognosis.

A-485, a selective and potent small-molecule inhibitor [25], targets specific tissues, thereby minimizing adverse effects on non-targeted tissues [41]. Studies have reported that A-485 has the potential to prevent

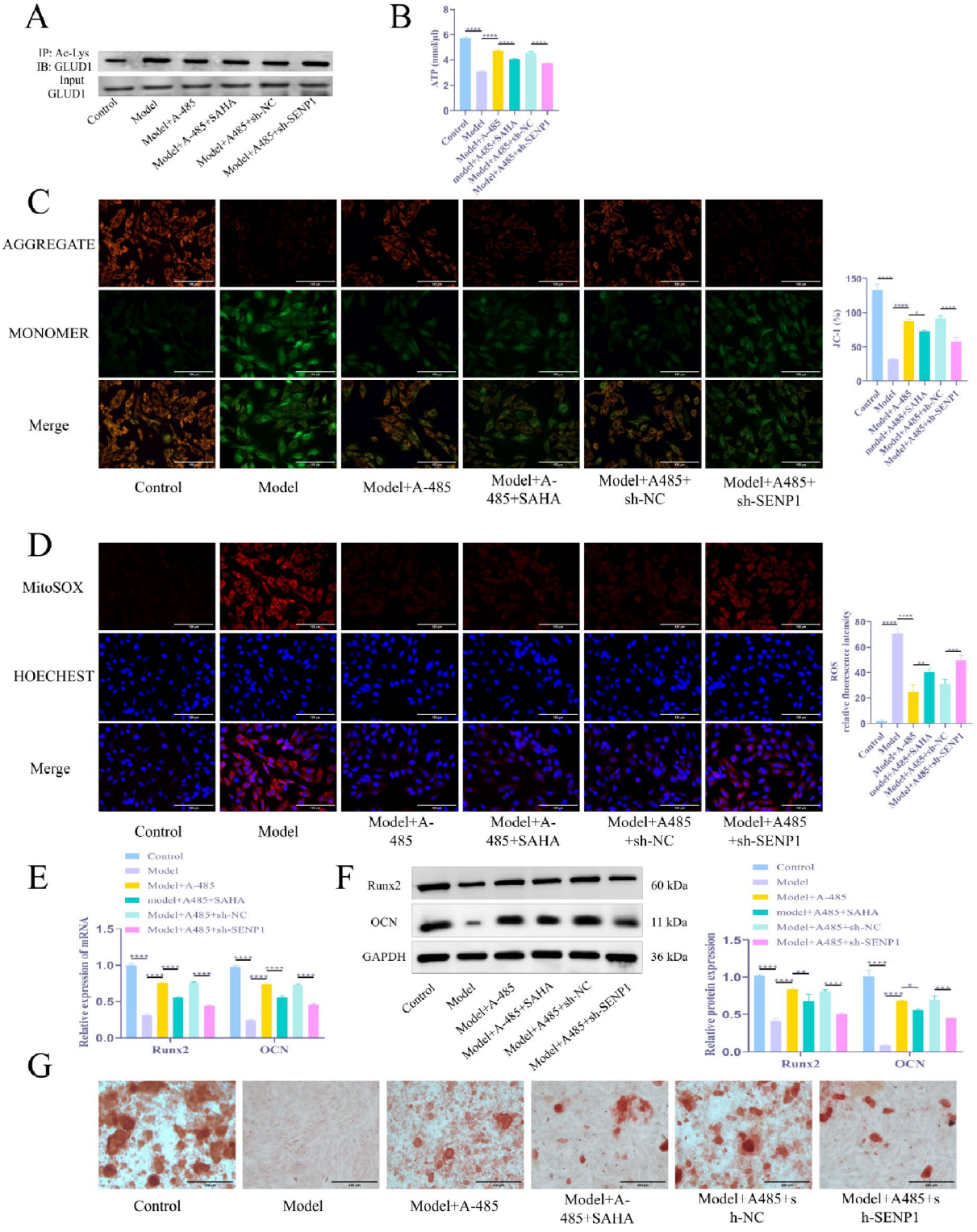

Fig. 6 The effects of A-485 on mitochondrial dysfunction, osteoblast differentiation, and calcification through modulating GLUD1 deacetylation via the SENP1-Sirt3 signal pathway. (**A**) Co-IP analysis of GLUD1 acetylation levels in MC3T3-E1 cells. (**B**) Measurement of ATP levels in MC3T3-E1 cells. (**C**) JC-1 staining to evaluate mitochondrial membrane potential (ΔΨm) in MC3T3-E1 cells. (**D**) Detection of intracellular ROS levels in MC3T3-E1 cells. (**E**) RT-qPCR analysis of Runx2 and OCN mRNA expression levels in MC3T3-E1 cells. (**F**) WB analysis of Runx2 and OCN protein expression levels in MC3T3-E1 cells. (**G**) Assessment of mineralization capability of MC3T3-E1 cells. $N = 3$; *, $p < 0.05$; ***, $p < 0.001$, ****, $p < 0.0001$

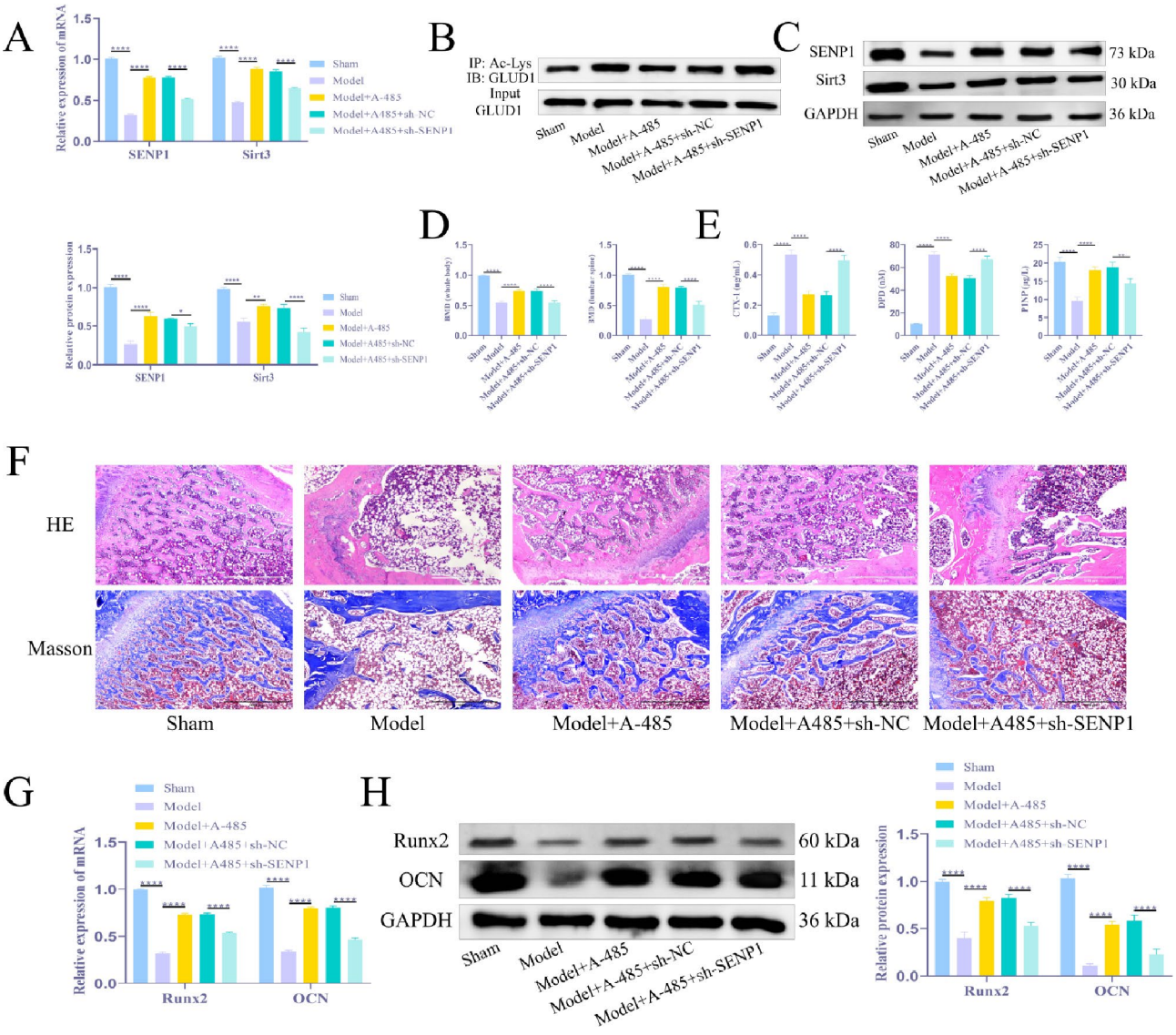

Fig. 7 The effect of A-485 on OP in ovariectomized rats via the SENP1-Sirt3 signal pathway. (**A**) RT-qPCR analysis of SENP1 and SIRT3 mRNA expression levels in rat cartilage tissue. (**B**) Co-IP analysis of acetylation levels of GLUD1. (**C**) WB analysis of SENP1 and SIRT3 protein expression levels in rat cartilage tissue. (**D**) Measurement of bone mineral density (BMD) in rat cartilage tissue. (**E**) Detection of CTX-1 and P1NP levels in rat serum, as well as DPD levels in urine. (**F**) HE and Masson's trichrome staining for histological observation of cartilage tissue. (**G**) RT-qPCR analysis of Runx2 and OCN mRNA expression levels in cartilage tissue. (**H**) WB analysis of Runx2 and OCN protein levels in cartilage tissue. $N = 6$; ns, $p > 0.05$; *, $p < 0.05$, **, $p < 0.01$; ****, $p < 0.0001$

postmenopausal OP and may be considered as a candidate molecule for OP treatment [42]. Our study also demonstrated that A-485 alleviated OP-related symptoms in ovariectomized rats, manifested by restoration of bone tissue damage, stimulation of osteoblast differentiation, and suppression of adipogenesis. These findings align with previous research, which has shown suppressive activities of A-485 in osteoclastogenesis and bone resorption [10]. Notably, its pleiotropic benefits extend beyond bone remodeling. A-485 concurrently inhibits lipogenesis in white adipose tissue and the liver by suppressing FOXO1 acetylation and promoting its degradation via a proteasome-dependent pathway [43]. This suggests that A-485 not only contributes to OP treatment but may also hold promise for addressing other bone-related conditions, such as fracture repair and bone tumors. Additionally, A-485 may exert indirect benefits for OP and associated metabolic disorders by regulating bone-fat balance and modulating other interconnected metabolic pathways.

Emerging evidence implicates mitochondrial dysfunction as a central driver of postmenopausal OP progression [44, 45]. OP-induced mitochondrial dysfunction can lead to elevated ROS, which in turn impaires osteoblast differentiation [46]. In mitochondria, $\Delta\psi m$ is critical for maintaining mitochondrial function and cellular

metabolism [47]. It drives ATP synthesis and regulates ROS production, and its changes directly reflect mitochondrial health and function [48]. Previous literature has established a link between mitochondrial dysfunction and protein acetylation modifications [49], with deacetylation of mitochondrial proteins shown to alleviate mitochondrial impairment [50]. Additionally, abnormal acetylation of mitochondrial proteins impairs mitochondrial energy metabolism, which can disrupt the function and metabolism of skeletal cells and tissues [51]. In our study, A-485 effectively alleviated mitochondrial dysfunction in OP-modeled MC3T3-E1 cells by selective deacetylation of mitochondrial proteins, while having no significant effect on the acetylation of non-mitochondrial protein. These findings are consistent with those of Weinert et al., who demonstrated that A-485 could regulate mitochondrial protein acetylation by inhibiting acetyltransferase activity [52]. These results suggest that A-485 has a regulatory effect on mitochondrial dysfunction and mitochondrial protein acetylation in OP. Notably, mitochondrial dysfunction has also been linked to other diseases such as Parkinson's disease [53], muscular dystrophy [54], diabetes mellitus [55], cardiovascular disease [56] and cancer [57]. Therefore, A-485 could also hold potential for breakthroughs in the treatment of these conditions.

GLUD1, an enzyme located in the mitochondrial matrix, plays a central role in regulating cellular energy metabolism, maintaining nitrogen homeostasis, and responding to changes in energy demand [58]. The acetylation status of GLUD1 influences mitochondrial function and bone metabolism, which in turn exacerbates or alleviates OP [59]. Therefore, modulating GLUD1 acetylation becomes a promising strategy for improving mitochondrial function and treating OP. In this study, we found that A-485 improved mitochondrial function and enhanced cell proliferation and mineralization by reducing the mitochondrial GLUD1 acetylation level in OP-modeled MC3T3-E1 cells, whereas acetylation activator SAHA reversesd this effect. Consistent with our study, the inhibitory role of A-485 in the acetylation level of mitochondrial proteins has also been demonstrated in previous publications [12]. However, to our knowledge, this study is the first to report the effect of A-485 on mitochondrial GLUD1 acetylation in the context of OP. Our results highlighted the critical role of GLUD1 acetylation in mitochondrial function and cellular metabolism, and demonstrated that A-485 alleviated the progression of OP by modulating the acetylation status of GLUD1. To conclude, this GLUD1-centric mechanism, unreported in prior OP studies, positions A-485 as an acetylation modulator with bone-specific efficacy. While our study focused on the effects of A-485 in modulating mitochondrial GLUD1 acetylation, further research is needed to explore other potential factors involved in this process and to assess the broader implications for bone health. Future studies could also investigate the potential clinical applications of A-485 and other acetylation modulators in the treatment of OP and other metabolic diseases.

The SENP1-Sirt3 signal pathway has been confirmed to be a critical regulator of mitochondrial GLUD1 deacetylation [20]. Cellular stress triggers a coordinated response wherein [60] SUMO-specific protease SENP1 translocates to mitochondria, catalyzing Sirt3 activation through de-SUMOylation, which is a prerequisite for its metabolic regulatory functions [61]. Sirt3, as a deacetylating enzyme, orchestrates cellular metabolism by modulating enzyme activities, including GLUD1 [62]. Despite these advances, the pathophysiological relevance of SENP1-Sirt3 signaling in OP has not been studied until now. Our study provided the first experimental evidence that the SENP1-Sirt3 pathway mediated GLUD1 deacetylation in postmenopausal OP pathogenesis. Crucially, we also demonstrated that A-485 significantly improved OP by activating this signal pathway, reducing GLUD1 acetylation levels, alleviating mitochondrial dysfunction, and ameliorating tissue and cellular damage. This novel pharmacodynamic profile distinguishes A-485 from conventional OP therapies, as no prior studies have reported its interaction with the SENP1-Sirt3-GLUD1 cascade. Although our data conclusively linked A-485's pharmacological effects to SENP1-Sirt3-mediated GLUD1 deacetylation, this study did not address the potential involvement of other signaling or their downstream factors in A-485's mechanisms. Moreover, the regulation of the SENP1-Sirt3 signal pathway involves multiple upstream signals, and its tissue-specific mechanisms are yet to be fully understood. Further studies should explore whether A-485's pleiotropic effects result from modulation of other signaling pathways, thereby necessitating systematic characterization of its multi-target potential for further investigation.

Our findings derive exclusively from cell models and animal experiments, lacking clinical data to validate the efficacy of A-485 in humans. Although the study focuses on the pharmacological effects of A-485 in OP treatment, its potential off-target effects and long-term safety remain insufficiently evaluated. To address these limitations, future research should further investigate the off-target effects of A-485 and prioritize long-term safety studies, particularly its potential impact on the liver and kidney, so as to provide a more comprehensive safety profile for clinical applications.

Conclusion

A-485 mitigates mitochondrial dysfunction while enhancing osteogenic differentiation and mineralization in ovariectomized rats by GLUD1 deacetylation through

activating the SENP1-Sirt3 signal pathway. Our findings may contribute to the development of new strategies for the clinical treatment of OP. A-485 and its analogs may represent promising pharmacological agents to improve the quality of life among OP patients.

Supplementary Information

The online version contains supplementary material available at https://doi.org/10.1186/s13018-025-05839-4.

Supplementary Material 1

Supplementary Material 2

Acknowledgements
We would like to express our gratitude to the participants who generously gave their time and effort to make this study possible.

Author contributions
All authors contributed to the study conception and design. Material preparation, data collection, and analysis were performed by Yinghong Ma, Xiaohua Zou, Qianhong Jian, Jiaxin Dong, Xianbing Huang, Yue Zhai, and Li Qian. The first draft of the manuscript was written by Yinghong Ma and all authors commented on previous versions of the manuscript. All authors read and approved the final manuscript.

Funding
The authors declare that no funds, grants, or other support were received during the preparation of this manuscript.

Data availability
No datasets were generated or analysed during the current study.

Declarations

Ethical approval
This study was performed in line with the principles of the Declaration of Helsinki. This study was approved by The Animal Ethics Committee of Guizhou Medical University (Ethics Approval Number:2023070110).

Consent for publication
Not applicable.

Competing interests
The authors declare no competing interests.

Author details
[1]College of Anesthesia, Guizhou Medical University, Guiyang, Guizhou 550000, China
[2]Department of Pain Medicine, Beijing Jishuitan Hospital Guizhou Hospital, Guiyang, Guizhou 550000, China
[3]Department of Anesthesiology, The Affiliated Hospital of Guizhou Medical University, Guiyang, Guizhou 550000, China
[4]No. 28 Guiyi Street, Yunyan District, Guiyang City, Guizhou Province, China
[5]123 Shachong South Road, Nanming District, Guiyang City, Guizhou Province, China

Received: 26 February 2025 / Accepted: 22 April 2025
Published online: 29 May 2025

References

1. Huidrom S, Beg MA, Masood T. Post-menopausal osteoporosis and probiotics. Curr Drug Targets. 2021;22(7):816–22. https://doi.org/10.2174/1389450121666201027124947.
2. Migliorini F, Colarossi G, Eschweiler J, Oliva F, Driessen A, Maffulli N. Anti-resorptive treatments for corticosteroid-induced osteoporosis: a bayesian network meta-analysis. Br Med Bull. 2022;143(1):46–56. https://doi.org/10.1093/bmb/ldac017.
3. Conti V, Russomanno G, Corbi G, Toro G, Simeon V, Filippelli W, et al. A polymorphism at the translation start site of the vitamin D receptor gene is associated with the response to anti-osteoporotic therapy in postmenopausal women from Southern Italy. Int J Mol Sci. 2015;16(3):5452–66. https://doi.org/10.3390/ijms16035452.
4. Migliorini F, Maffulli N, Colarossi G, Eschweiler J, Tingart M, Betsch M. Effect of drugs on bone mineral density in postmenopausal osteoporosis: a bayesian network meta-analysis. J Orthop Surg Res. 2021;16(1):533. https://doi.org/10.1186/s13018-021-02678-x.
5. Martiniakova M, Babikova M, Omelka R. Pharmacological agents and natural compounds: available treatments for osteoporosis. J Physiol Pharmacol. 2020;71(3). https://doi.org/10.26402/jpp.2020.3.01.
6. Migliorini F, Giorgino R, Hildebrand F, Spiezia F, Peretti GM, Alessandri-Bonetti M, et al. Fragility fractures: risk factors and management in the elderly. Med (Kaunas). 2021;57(10). https://doi.org/10.3390/medicina57101119.
7. Skjodt MK, Frost M, Abrahamsen B. Side effects of drugs for osteoporosis and metastatic bone disease. Br J Clin Pharmacol. 2019;85(6):1063–71. https://doi.org/10.1111/bcp.13759.
8. Ji C, Xu W, Ding H, Chen Z, Shi C, Han J, et al. The p300 inhibitor A-485 exerts antitumor activity in growth hormone pituitary adenoma. J Clin Endocrinol Metab. 2022;107(6):e2291–300. https://doi.org/10.1210/clinem/dgac128.
9. Zhang L, Sheng C, Zhou F, Zhu K, Wang S, Liu Q, et al. CBP/p300 HAT maintains the gene network critical for beta cell identity and functional maturity. Cell Death Dis. 2021;12(5):476. https://doi.org/10.1038/s41419-021-03761-1.
10. Huo S, Liu X, Zhang S, Lyu Z, Zhang J, Wang Y, et al. p300/CBP inhibitor A-485 inhibits the differentiation of osteoclasts and protects against osteoporotic bone loss. Int Immunopharmacol. 2021;94:107458. https://doi.org/10.1016/j.intimp.2021.107458.
11. Zhou XR, Li X, Liao LP, Han J, Huang J, Li JC, et al. P300/CBP Inhibition sensitizes mantle cell lymphoma to PI3Kdelta inhibitor idelalisib. Acta Pharmacol Sin. 2022;43(2):457–69. https://doi.org/10.1038/s41401-021-00643-2.
12. Shi J, Wang QH, Wei X, Huo B, Ye JN, Yi X, et al. Histone acetyltransferase P300 deficiency promotes ferroptosis of vascular smooth muscle cells by activating the HIF-1alpha/HMOX1 axis. Mol Med. 2023;29(1):91. https://doi.org/10.1186/s10020-023-00694-7.
13. Piot L, Heroven C, Bossi S, Zamith J, Malinauskas T, Johnson C, et al. GluD1 binds GABA and controls inhibitory plasticity. Science. 2023;382(6677):1389–94. https://doi.org/10.1126/science.adf3406.
14. Shang M, Cappellesso F, Amorim R, Serneels J, Virga F, Eelen G, et al. Macrophage-derived glutamine boosts satellite cells and muscle regeneration. Nature. 2020;587(7835):626–31. https://doi.org/10.1038/s41586-020-2857-9.
15. Lu CW, Lin TY, Pan TL, Wang PW, Chiu KM, Lee MY, et al. Asiatic acid prevents cognitive deficits by inhibiting Calpain activation and preserving synaptic and mitochondrial function in rats with Kainic acid-Induced seizure. Biomedicines. 2021;9(3). https://doi.org/10.3390/biomedicines9030284.
16. Yoh K, Ikeda K, Horie K, Inoue S. Roles of Estrogen, Estrogen receptors, and Estrogen-Related receptors in skeletal muscle: regulation of mitochondrial function. Int J Mol Sci. 2023;24(3). https://doi.org/10.3390/ijms24031853.
17. Yang T, Chen W, Gan K, Wang C, Xie X, Su Y, et al. Myrislignan targets extracellular signal-regulated kinase (ERK) and modulates mitochondrial function to dampen osteoclastogenesis and ovariectomy-induced osteoporosis. J Transl Med. 2023;21(1):839. https://doi.org/10.1186/s12967-023-04706-2.
18. Zhang P, Wu H, Lou H, Zhou J, Hao J, Lin H, et al, et al. Baicalin attenuates diabetic cardiomyopathy in vivo and in vitro by inhibiting autophagy and cell death through SENP1/SIRT3 signaling pathway activation. Antioxid Redox Signal. 2024. https://doi.org/10.1089/ars.2023.0457.
19. Chen DD, Shi Q, Liu X, Liang DL, Wu YZ, Fan Q, et al. Aberrant SENP1-SUMO-Sirt3 signaling causes the disturbances of mitochondrial deacetylation and oxidative phosphorylation in Prion-Infected animal and cell models. ACS Chem Neurosci. 2023;14(9):1610–21. https://doi.org/10.1021/acschemneuro.2c00786.
20. Zhou W, Hu G, He J, Wang T, Zuo Y, Cao Y, et al. SENP1-Sirt3 signaling promotes alpha-ketoglutarate production during M2 macrophage polarization. Cell Rep. 2022;39(2):110660. https://doi.org/10.1016/j.celrep.2022.110660.
21. Guhathakurta S, Erdogdu NU, Hoffmann JJ, Grzadzielewska I, Schendzielorz A, Seyfferth J, et al. COX17 acetylation via MOF-KANSL complex promotes mitochondrial integrity and function. Nat Metab. 2023;5(11):1931–52. https://doi.org/10.1038/s42255-023-00904-w.

22. Liu J, Gao Z, Liu X. Mitochondrial dysfunction and therapeutic perspectives in osteoporosis. Front Endocrinol (Lausanne). 2024;15:1325317. https://doi.org/10.3389/fendo.2024.1325317.
23. Chen C, Chen B, Lin Y, He Q, Yang J, Xiao J, et al. Cardamonin attenuates iron overload-induced osteoblast oxidative stress through the HIF-1alpha/ROS pathway. Int Immunopharmacol. 2024;142(Pt A):112893. https://doi.org/10.1016/j.intimp.2024.112893.
24. Fang Y, Zhang J, Zhu S, He M, Ma S, Jia Q, et al. Berberine ameliorates ovariectomy-induced anxiety-like behaviors by enrichment in equol generating gut microbiota. Pharmacol Res. 2021;165:105439. https://doi.org/10.1016/j.phrs.2021.105439.
25. Peng J, Li J, Huang J, Xu P, Huang H, Liu Y, et al. p300/CBP inhibitor A-485 alleviates acute liver injury by regulating macrophage activation and polarization. Theranostics. 2019;9(26):8344–61. https://doi.org/10.7150/thno.30707.
26. Schiavi J, Fodera DM, Brennan MA, McNamara LM. Estrogen depletion alters osteogenic differentiation and matrix production by osteoblasts in vitro. Exp Cell Res. 2021;408(1):112814. https://doi.org/10.1016/j.yexcr.2021.112814.
27. Amaroli A, Pasquale C, Zekiy A, Utyuzh A, Benedicenti S, Signore A et al. Photobiomodulation and oxidative stress: 980 nm diode laser light regulates mitochondrial activity and reactive oxygen species production. Oxid Med Cell Longev. 2021:6626286. https://doi.org/10.1155/2021/6626286
28. Tang F, Wang S, Zhao H, Xia D, Dong X. Mendelian randomization analysis does not reveal a causal influence of mental diseases on osteoporosis. Front Endocrinol (Lausanne). 2023;14:1125427. https://doi.org/10.3389/fendo.2023.1125427.
29. Kanis JA, Cooper C, Rizzoli R, Reginster JY et al. Scientific Advisory Board of the European Society for C, Economic Aspects of O (2019) European guidance for the diagnosis and management of osteoporosis in postmenopausal women. Osteoporos Int. 2019;30(1):3–44.https://doi.org/10.1007/s00198-018-4704-5
30. Migliorini F, Maffulli N, Spiezia F, Peretti GM, Tingart M, Giorgino R. Potential of biomarkers during Pharmacological therapy setting for postmenopausal osteoporosis: a systematic review. J Orthop Surg Res. 2021;16(1):351. https://doi.org/10.1186/s13018-021-02497-0.
31. Huang F, Wang Y, Liu J, Cheng Y, Zhang X, Jiang H. Asperuloside alleviates osteoporosis by promoting autophagy and regulating Nrf2 activation. J Orthop Surg Res. 2024;19(1):855. https://doi.org/10.1186/s13018-024-05320-8.
32. Andersen MO, Andresen AK, Hartvigsen J, Hermann AP, Sorensen J, Carreon LY. Vertebroplasty for painful osteoporotic vertebral compression fractures: a protocol for a single-center doubled-blind randomized sham-controlled clinical trial. VOPE2. J Orthop Surg Res. 2024;19(1):813. https://doi.org/10.1186/s13018-024-05301-x.
33. Wu D, Cline-Smith A, Shashkova E, Perla A, Katyal A, Aurora R. T-Cell mediated inflammation in postmenopausal osteoporosis. Front Immunol. 2021;12:687551. https://doi.org/10.3389/fimmu.2021.687551.
34. Migliorini F, Maffulli N, Spiezia F, Tingart M, Maria PG, Riccardo G. Biomarkers as therapy monitoring for postmenopausal osteoporosis: a systematic review. J Orthop Surg Res. 2021;16(1):318. https://doi.org/10.1186/s13018-021-02474-7.
35. Shen L, Yang H, Zhou F, Jiang T, Jiang Z. Risk factors of short-term residual low back pain after PKP for the first thoracolumbar osteoporotic vertebral compression fracture. J Orthop Surg Res. 2024;19(1):792. https://doi.org/10.1186/s13018-024-05295-6.
36. Leeyaphan J, Rojjananukulpong K, Intarasompun P, Peerakul Y. Simple clinical predictors for making directive decisions in osteoporosis screening for women: a cross-sectional study. J Orthop Surg Res. 2024;19(1):789. https://doi.org/10.1186/s13018-024-05287-6.
37. Ayers C, Kansagara D, Lazur B, Fu R, Kwon A, Harrod C. Effectiveness and safety of treatments to prevent fractures in people with low bone mass or primary osteoporosis: A living systematic review and network Meta-analysis for the American college of physicians. Ann Intern Med. 2023;176(2):182–95. https://doi.org/10.7326/M22-0684.
38. Migliorini F, Colarossi G, Baroncini A, Eschweiler J, Tingart M, Maffulli N. Pharmacological management of postmenopausal osteoporosis: a level I evidence Based - Expert opinion. Expert Rev Clin Pharmacol. 2021;14(1):105–19. https://doi.org/10.1080/17512433.2021.1851192.
39. Handel MN, Cardoso I, von Bulow C, Rohde JF, Ussing A, Nielsen SM, et al. Fracture risk reduction and safety by osteoporosis treatment compared with placebo or active comparator in postmenopausal women: systematic review, network meta-analysis, and meta-regression analysis of randomised clinical trials. BMJ. 2023;381:e068033. https://doi.org/10.1136/bmj-2021-068033.
40. Bao X, Liu C, Liu H, Wang Y, Xue P, Li Y. Association between polymorphisms of glucagon-like peptide-1 receptor gene and susceptibility to osteoporosis in Chinese postmenopausal women. J Orthop Surg Res. 2024;19(1):869. https://doi.org/10.1186/s13018-024-05361-z.
41. Mastracchio A, Lai C, Digiammarino E, Ready DB, Lasko LM, Bromberg KD, et al. Discovery of a potent and selective covalent p300/CBP inhibitor. ACS Med Chem Lett. 2021;12(5):726–31. https://doi.org/10.1021/acsmedchemlett.0c00654.
42. Zhang L, Zhu K, Xu J, Chen X, Sheng C, Zhang D, et al. Acetyltransferases CBP/p300 control transcriptional switch of beta-Catenin and Stat1 promoting osteoblast differentiation. J Bone Min Res. 2023;38(12):1885–99. https://doi.org/10.1002/jbmr.4925.
43. Zhou F, Liu Q, Zhang L, Zhu Q, Wang S, Zhu K, et al. Selective Inhibition of CBP/p300 HAT by A-485 results in suppression of lipogenesis and hepatic gluconeogenesis. Cell Death Dis. 2020;11(9):745. https://doi.org/10.1038/s41419-020-02960-6.
44. Yan C, Shi Y, Yuan L, Lv D, Sun B, Wang J, et al. Mitochondrial quality control and its role in osteoporosis. Front Endocrinol (Lausanne). 2023;14:1077058. https://doi.org/10.3389/fendo.2023.1077058.
45. Zeng Z, Zhou X, Wang Y, Cao H, Guo J, Wang P, et al. Mitophagy-a new target of bone disease. Biomolecules. 2022;12(10). https://doi.org/10.3390/biom12101420.
46. Cai W, Zhang J, Yu Y, Ni Y, Wei Y, Cheng Y, et al. Mitochondrial transfer regulates cell fate through metabolic remodeling in osteoporosis. Adv Sci (Weinh). 2023;10(4):e2204871. https://doi.org/10.1002/advs.202204871.
47. Tomita K, Kuwahara Y, Igarashi K, Roudkenar MH, Roushandeh AM, Kurimasa A, et al. Mitochondrial dysfunction in diseases, longevity, and treatment resistance: tuning mitochondria function as a therapeutic strategy. Genes (Basel). 2021;12(9). https://doi.org/10.3390/genes12091348.
48. Mills EL, Kelly B, Logan A, Costa ASH, Varma M, Bryant CE, et al. Succinate dehydrogenase supports metabolic repurposing of mitochondria to drive inflammatory macrophages. Cell. 2016;167(2):457–70. https://doi.org/10.1016/j.cell.2016.08.064.
49. Samuvel DJ, Krishnasamy Y, Li L, Lemasters JJ, Chou CJ, Zhong Z. LP342, a novel histone deacetylase inhibitor, decreases nitro-oxidative stress, mitochondrial dysfunction and hepatic ischaemia/reperfusion injury in mice. RPS Pharm Pharmacol Rep. 2023;2(2):rqad013. https://doi.org/10.1093/rpsppr/rqad013.
50. Tomczyk MM, Cheung KG, Xiang B, Tamanna N, Fonseca Teixeira AL, Agarwal P, et al. Mitochondrial Sirtuin-3 (SIRT3) prevents Doxorubicin-Induced dilated cardiomyopathy by modulating protein acetylation and oxidative stress. Circ Heart Fail. 2022;15(5):e008547. https://doi.org/10.1161/CIRCHEARTFAILURE.121.008547.
51. Chen X, Ji Y, Liu R, Zhu X, Wang K, Yang X, et al. Mitochondrial dysfunction: roles in skeletal muscle atrophy. J Transl Med. 2023;21(1):503. https://doi.org/10.1186/s12967-023-04369-z.
52. Weinert BT, Narita T, Satpathy S, Srinivasan B, Hansen BK, Scholz C, et al. Time-Resolved analysis reveals rapid dynamics and broad scope of the CBP/p300 acetylome. Cell. 2018;174(1):231–44. https://doi.org/10.1016/j.cell.2018.04.033.
53. Eldeeb MA, Thomas RA, Ragheb MA, Fallahi A, Fon EA. Mitochondrial quality control in health and in Parkinson's disease. Physiol Rev. 2022;102(4):1721–55. https://doi.org/10.1152/physrev.00041.2021.
54. Dubinin MV, Mikheeva IB, Stepanova AE, Igoshkina AD, Cherepanova AA, Semenova AA, et al. Mitochondrial transplantation therapy ameliorates muscular dystrophy in Mdx mouse model. Biomolecules. 2024;14(3). https://doi.org/10.3390/biom14030316.
55. Shan Z, Fa WH, Tian CR, Yuan CS, Jie N. Mitophagy and mitochondrial dynamics in type 2 diabetes mellitus treatment. Aging. 2022;14(6):2902–19. https://doi.org/10.18632/aging.203969.
56. Li A, Gao M, Liu B, Qin Y, Chen L, Liu H, et al. Mitochondrial autophagy: molecular mechanisms and implications for cardiovascular disease. Cell Death Dis. 2022;13(5):444. https://doi.org/10.1038/s41419-022-04906-6.
57. Luo Y, Ma J, Lu W. The significance of mitochondrial dysfunction in cancer. Int J Mol Sci. 2020;21(16). https://doi.org/10.3390/ijms21165598.
58. Wu Z, Li N, Gao Y, Cao L, Yao X, Peng Q. Glutamine metabolism-related genes and immunotherapy in nonspecific orbital inflammation were validated using bioinformatics and machine learning. BMC Genomics. 2024;25(1):71. https://doi.org/10.1186/s12864-023-09946-6.

59. Fan M, Shi H, Yao H, Wang W, Zhang Y, Jiang C, et al. Glutamate regulates gliosis of BMSCs to promote ENS regeneration through alpha-KG and H3K9/H3K27 demethylation. Stem Cell Res Ther. 2022;13(1):255. https://doi.org/10.1186/s13287-022-02936-7.
60. He J, Cheng J, Wang T. SUMOylation-Mediated response to mitochondrial stress. Int J Mol Sci. 2020;21(16). https://doi.org/10.3390/ijms21165657.
61. Cheng A, Yang Y, Zhou Y, Maharana C, Lu D, Peng W, et al. Mitochondrial SIRT3 mediates adaptive responses of neurons to exercise and metabolic and excitatory challenges. Cell Metab. 2016;23(1):128–42. https://doi.org/10.1016/j.cmet.2015.10.013.
62. Blander G, Guarente L. The Sir2 family of protein deacetylases. Annu Rev Biochem. 2004;73:417–35. https://doi.org/10.1146/annurev.biochem.73.011303.073651.

Publisher's note